# Prediction of Punching Shear Strength of Reinforced Concrete Flat Slab by ANSYS

Mohammed Ali Ihsan Saber[1]

[1] Civil Engineering Department, University of Salahaddin, Erbil, Iraq
Correspondence: Mohammed Ali Ihsan Saber, University of Salahaddin, Erbil, Iraq.
Email: mohammed.saber@su.edu.krd

Received: April 7, 2018 Accepted: May 23, 2018 Online Published: June 1, 2018

doi: 10.23918/eajse.v3i3p42

**Abstract: In this study, finite element software ANSYS is used to model a three-dimensional finite element (FE) model to study the punching shear behavior of normal (NSC) and high strength concrete (HSC) flat plate slabs. The FE model is verified through application to experimental models, and high accuracy was obtained. The FE model was used to determine cracking load, ultimate load capacity, load-deflection curves, stress-strain relationship, and failure modes for all tested slabs. Results of nine NSC and HSC flat plate slabs were tested under punching loading. The main variables considered were the concrete compressive strength varied from 40 to 110 MPa, and column eccentricities 0%, 50% and 100% of column size. The behaviors of the finite element models showed good agreement with those got from experimental results in all linear, nonlinear and final failure stages.**

**Keywords: Finite Element model, Flat Plate Slabs, Punching Shear**

## 1. Introduction

The flat plate is (also called as slab-column structure) a competitive and common structural system for cast in place slabs since no column drop panels, capitals, or beams, are involved which effectively reduce stories height and allow a full use of the available space, which has an economic advantage. One of the most critical analysis issues in the design of reinforced concrete flat plate (RCFP) slabs is the punching shear in the zones around the columns. Column tends to penetrate through the RCFP, flat slabs and footings because of the high shear stresses, around the columns perimeter. Both beam (one way) and punching (two way) type Shear failure may be considered more dangerous than flexural failure because of the lack of predicting shear punching failure, which occurs suddenly without any advanced warning. This kind of shear failure may significantly reduce the whole structural resistance against gravity loads, and lead to the overall collapse of the structure. The present research aims at achieving the following objectives:

1. To develop an FE model to study the behavior of RCFP under punching loads using finite element software ANSYS and compare it with experimental test results.
2. To determine the complete load-deflection response of RCFP and predict the ultimate load capacity of such structures.
3. To study the effect of flexural and shear reinforcement on the punching shear strength.

The FE program (ANSYS) is capable of devoted numerical models for the linear and nonlinear response of concrete under static and dynamic loading. In order to verify the initial FE model, experimental test result was used.

## 2. Finite Element Modeling

The meshing of the FE model is one of the primary steps in which, the FE model is divided into a number of smaller elements. In order to obtain a convergence of results in the model, a suitable number of elements must be used. This is can be achieved when the decreasing of the mesh size has an insignificant effect on the results. Optimum meshing size was calculated graphically by applying a constant load and it plots the maximum deflection versus mesh size as shown in Figure 1. The Figure shows an insignificant difference in deflection when mesh size in the model decreased from 25 mm to 10 mm. therefore, the 25 mm mesh size model was selected for the model slabs.

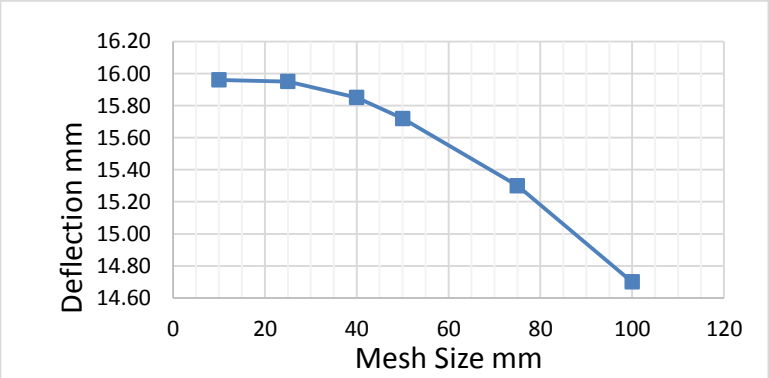


Figure 1: optimum meshing size of the FE model

## 3. Methodology and the FE Analytical Model Data

The concrete was modeled using ANSYS element type (Solid65). Solid65 is an eight nodes element, having three degrees of freedom at each node in the nodal x, y, and z directions. The element has the ability to express cracking, plastic deformation and crushing in three orthogonal directions. Figure 2 shows a graphical description of the element. The ANSYS element (Link180) was used to model the reinforcement (main flexural and column tie bars). Element Link180 is a three-dimensional spar element. It has two nodes with three degrees of freedom at each node. The element has the capability of elastic and plastic deformation, Figure 3 shows the geometry and node locations of the element. The steel plates under loading area were modeled using an eight-node solid element, (Solid 185). The element has three degrees of freedom at each node in the nodal x, y, and z directions. The node locations and geometry for the element are shown in Figure 4 (ANSYS, Manual, 2016).

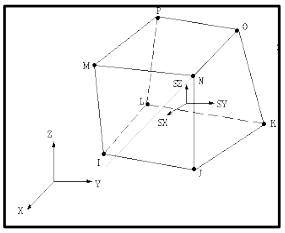

Figure 2: Solid 65 element

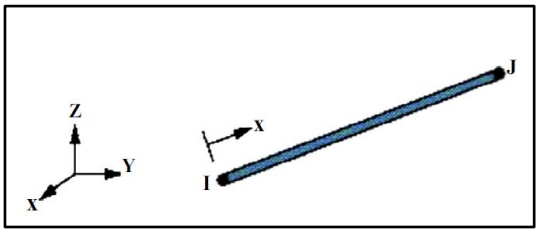


Figure 3: Link 180 element

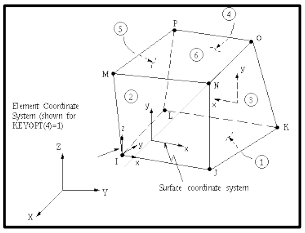

Figure 4: Solid185 element

In order to model concrete in ANSYS material properties, data must be input such as Elastic modulus (*Ec*), ultimate uniaxial compressive strength ($f_c$), ultimate tensile strength (modulus of rupture, $f_t$), Poisson's ratio ($v$), and uniaxial compressive stress-strain relationship for concrete. A summary of the concrete properties are used in this study is shown in Table 1.

Table 1: Concrete Properties

| $f_c$ (MPa) | 40 | | $f_c$ (MPa) | 75 | | $f_c$ (MPa) | 110 | |
|---|---|---|---|---|---|---|---|---|
| $f_t$ (MPa) | 2.5 | | $f_t$ (MPa) | 3.5 | | $f_t$ (MPa) | 4.2 | |
| Linear Isotropic | | | Linear Isotropic | | | Linear Isotropic | | |
| $E_c$ (GPa) | 30000 | | $E_c$ (GPa) | 41.1 | | $E_c$ (GPa) | 49.8 | |
| $v$ | 0.18 | | $v$ | 0.18 | | $v$ | 0.18 | |
| Multi - Linear Isotropic | | | Multi - Linear Isotropic | | | Multi - Linear Isotropic | | |
| Point | Strain mm/mm | Stres | Point | Strain mm/mm | Stres | Point | Strain mm/mm | Stres |
| 1 | 0.0004 | 12.0 | 1 | 0.0005 | 22.5 | 1 | 0.0007 | 33.0 |
| 2 | 0.0010 | 21.2 | 2 | 0.0013 | 39.9 | 2 | 0.0016 | 58.5 |
| 3 | 0.0015 | 29.2 | 3 | 0.0021 | 54.7 | 3 | 0.0025 | 80.3 |
| 4 | 0.0021 | 35.2 | 4 | 0.0029 | 66.0 | 4 | 0.0035 | 96.9 |
| 5 | 0.0027 | 40.0 | 5 | 0.0036 | 75.0 | 5 | 0.0044 | 110. |

In the nonlinear stages of reinforced concrete, the coefficient of shear transfer ($\beta_t$), should be assumed. This coefficient characterizes the conditions of the crack face. $\beta_t$ values range from 0.0 (smooth crack, zero shear transfer) to 1.0 (rough crack, no loss of shear) (ANSYS 2016). In this study, based on a number of trials a value of 0.35 was used for $\beta_t$, which resulted in quite good predictions. Values less than 0.3 caused problems in divergence at low loading stages. To create the uniaxial compressive stress-strain curve for concrete, numerical expressions Equation (1) and (2) (Desayi & Krishan, 1964), were used along with Equation (3) (Gere & Timoshenko, 1997).

$$f = \frac{E_c\,\varepsilon}{1 + \left(\frac{\varepsilon}{\varepsilon_o}\right)^2} \qquad (1)$$

$$\varepsilon_o = \frac{2f_c'}{E_c} \qquad (2)$$

$$E_c = \frac{f}{\varepsilon} \qquad (3)$$

$f = Stress\ corresponding\ to\ any\ strain\ \varepsilon$
$\varepsilon = Strain\ corresponding\ to\ \ stress\ f$
$\varepsilon_o = Strain\ at\ ultimate\ compressive\ stress, f_c'$

The typical and simplified uniaxial compressive stress-strain curve that was used in this study is shown in Figure 5 and 6 respectively. The stress-strain relationship for each flat slab model is built using six points linked by straight lines. The multilinear curve starts with zero stress-strain points. The first Point (No.1) was computed at ($0.30f'_c$) stress, using Equation (3) from the linear stress-strain relationship of the concrete. Points No. 2, 3, and 4 were calculated from Equation (1), in which ($\varepsilon_0$) is obtained from Equation (2). Point No. 5 is at ($\varepsilon_0$) and $f'_c$. The stress-strain relationship after Point No. 5 was assumed to be perfect plastic behavior.

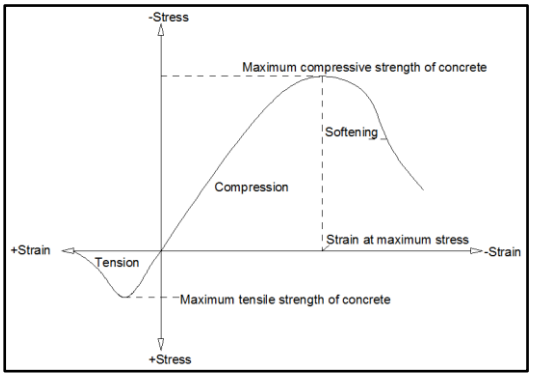


Figure 5: Typical Tensile and Compressive Stress Strain Curve for Concrete (Timoshenko & Gere, 1997)

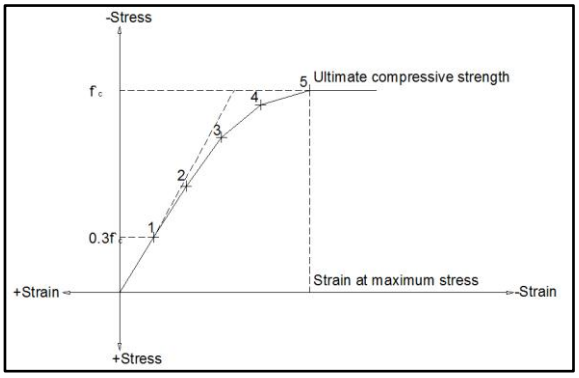


Figure 6: Simplified uniaxial compressive stress-stain relationship for concrete

The real, uniaxial stress-strain relationship for steel was modified to an elastic-perfect plastic behavior with strain hardening. The stress-strain relation in tension and in compression was assumed to be identical, as shown in Figure 7. In this study, the properties of the steel reinforcement were yielding stress, $f_y$= 420 MPa, modulus of elasticity, Es = 200 GPa, and Poisson's ratio = 0.3.

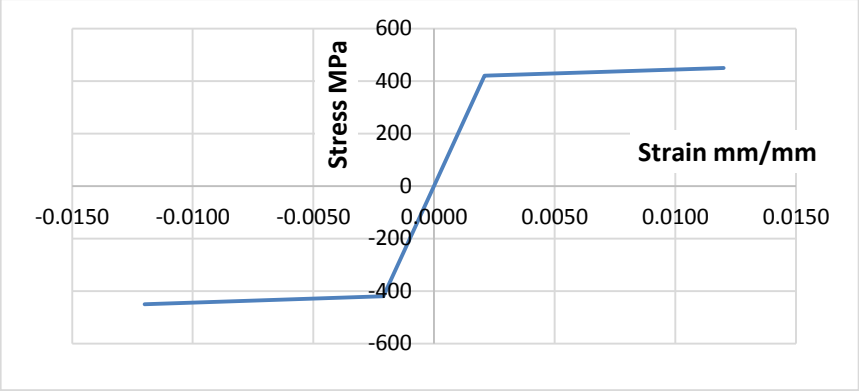


Figure 7: Idealized Stress-Strain Relationship for steel

## 4. Geometry of the Finite Element Model

The test series consists of nine reinforced concrete square slabs. The total side length of the slab specimens equals to 1000 mm, from which span of 850 mm is taken with a slab thickness of 55 mm and effective depth, $d_{avg}$ of 39 mm. In order to simulate the slab-column connection realistically, square cross-section column stubs (120 mm × 120 mm) were modeled on the tension (lower) and compression (upper) sides of the slabs that extend 150 mm from lower and 300 mm from the upper surface. All slabs were provided with φ 8 mm diameter orthogonal flexural reinforcement spaced at 65 mm c/c. Figure 8 and Table 2, give the properties and details of the tested specimens (Darwish & Yaseen, 2006). Tested slabs are divided into three series (N, H1, H2), with three different concrete nominal compressive strength levels, namely NSC ($f'_c$ = 40 MPa), HSC ($f'_c$ = 75 MPa) and ultra-HSC ($f'_c$ = 110 MPa). These series were used to study the effect of loading eccentricities: zero, one-half, and one time the column dimensioned (0, 60, and 120 mm). In order to minimize the required disk space and running time for computer computation process, only one-quarter of the full slab was used for modeling due to the symmetry of the tested slabs.

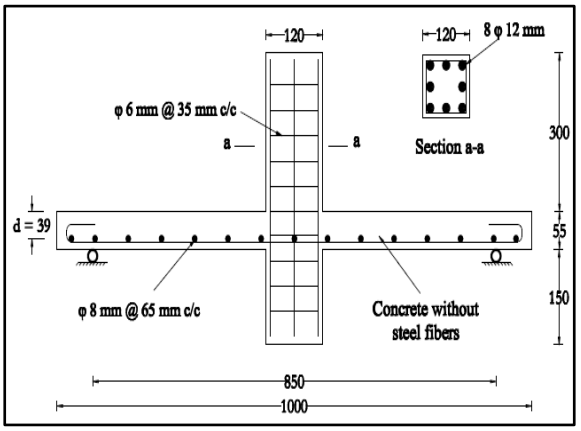


Figure 8: Details of the tested slabs

Table 2: Flat plate slabs specimens groups

| Specimen No. | $f'_c$ (MPa) | e/c | Eccentricity e (mm) |
|---|---|---|---|
| N-0 | 40 | 0 | 0 |
| N-60 | | 0.5 | 60 |
| N-120 | | 1.0 | 120 |
| H1-0 | 75 | 0 | 0 |
| H1-60 | | 0.5 | 60 |
| H1-120 | | 1.0 | 120 |
| H2-0 | 110 | 0 | 0 |
| H2-60 | | 0.5 | 60 |
| H2-120 | | 1.0 | 120 |

## 5. Loading and Boundary Conditions

In order to get a unique solution for the model, a specific displacement boundary conditions were used, to enforce the model to behave in the same manner as the experimental specimens. These boundary conditions should be applied at the symmetry loadings and supports locations. First, the boundary conditions for symmetry were set. The model has two planes of symmetry. Figure 9 shows all the applied boundary conditions for end supports and planes of symmetry. The section in which defines the plane of symmetry is a vertical plane through the center of the slab at mid-span. In order to model the symmetry condition, all the nodes in the plane of symmetry, restrained in the longitudinal direction. Therefore, the displacement along the X-direction and Z-direction for all the nodes in these planes were equaled to zero, (UX = 0, UZ = 0). The end support was modeled as a roller support. A set of nodes on a single line of the concrete plate element were restrained in the Y and Z directions, by gave constant values of zero (UY=0, UZ=0), so as, the slab will be free to rotate at the support. The applied load, P, is applied across all the entire nodes of the column top plane.

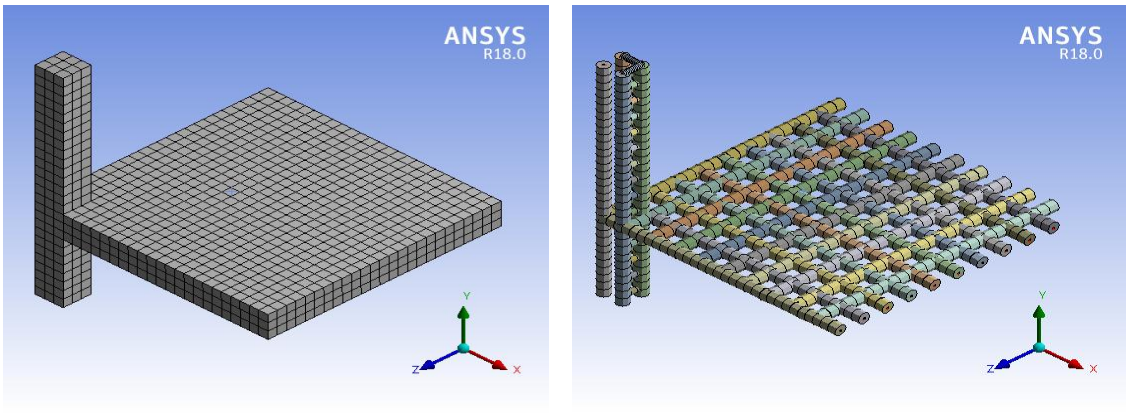


Figure 9: The FE model of the flat plate slab, showing mesh and boundary conditions

## 6. Experimental and Theoretical Results Comparison

To carry out finite element analysis in order to predict the behavior of any structure, it is essential to verify the developed model against some theoretical or test results to ensure that the developed

model is tracing the actual response closely. Results from the nonlinear finite element analysis are compared with the test results obtained from Darwish and Yaseen (2006) to ensure the acceptability of the obtained results in Table 3. Comparative load-deflection response for the test and FE results are shown in Figure 10 and 11 for N-0 and H1-120, similar figures can be obtained for other Flat slabs.

Table 3: Slab details with theoretical and experimental load and displacements results

| Specimen No. | e/c | $P_{cr\ Exp.}$ (kN) | $P_{cr\ ANSYS}$ (kN) | $\frac{Pcr\ Ex}{Pcr\ ANS}$ | $P_{u\ Exp.}$ (kN) | $P_{u\ ANSYS}$ (kN) | $\frac{Pu\ Ex}{Pu\ AN}$ | $\Delta_{u\ Exp.}$ (mm) | $\Delta_{u\ ANSYS}$ (mm) | $\frac{\Delta u\ Exp.}{\Delta u\ ANSY}$ |
|---|---|---|---|---|---|---|---|---|---|---|
| N-0 | 0 | 13.73 | 7.36 | 187% | 98.07 | 96.00 | 102% | 12.73 | 13.63 | 93% |
| N-60 | 0.5 | 11.28 | 7.32 | 154% | 81.40 | 81.68 | 100% | 10.18 | 10.35 | 98% |
| N-120 | 1 | 10.30 | 6.46 | 159% | 64.97 | 64.80 | 100% | 9.69 | 7.83 | 124% |
| H1-0 | 0 | 16.67 | 6.91 | 241% | 112.78 | 112.80 | 100% | 13.30 | 13.37 | 99% |
| H1-60 | 0.5 | 13.80 | 6.24 | 221% | 92.92 | 92.92 | 100% | 11.86 | 11.36 | 104% |
| H1-120 | 1 | 12.75 | 5.53 | 231% | 71.10 | 71.00 | 100% | 10.32 | 9.90 | 104% |
| H2-0 | 0 | 17.23 | 6.60 | 261% | 118.17 | 118.80 | 99% | 15.23 | 15.95 | 95% |
| H2-60 | 0.5 | 15.20 | 6.23 | 244% | 99.05 | 98.40 | 101% | 13.15 | 10.67 | 123% |
| H2-120 | 1 | 14.83 | 5.98 | 248% | 79.92 | 80.00 | 100% | 11.94 | 8.46 | 141% |

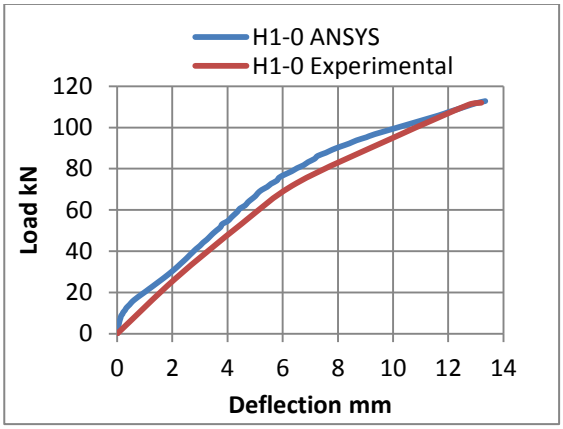


Figure 10: theoretical and deflection load-Deflection curve for H1-0

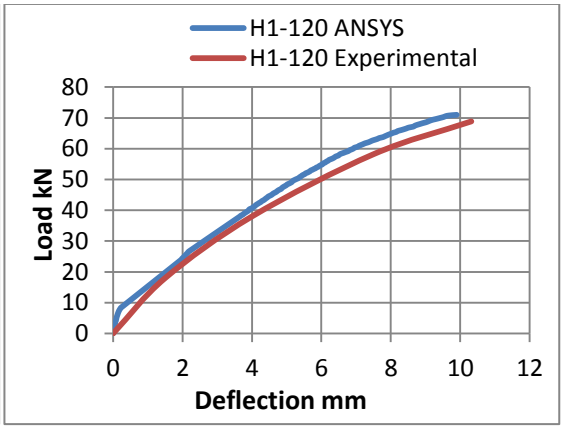


Figure 11: theoretical and deflection load-Deflection curve for H1-120

## 7. Load-Deflection Response

Table 3 presents all the results, theoretical and experimental. Figures 12, 13, and 14 show the axial punching load-deflection curves for N, H1 and H2 flat slabs groups, respectively. The predicted load-deflection curve from the FE model shows good agreement with experimental work. Generally, the load-deflection curves obtained from FE model were more stiffener than the curves obtained from the experimental in all loading stages (pre-cracking and post-cracking). This is due to:

1. In real casted concrete many types of micro-cracks may produce due to drying shrinkage, and handling, causing a significant reduction in the slab stiffness, while this is not presented in the FE model.
2. A full bond between the steel reinforcement and the concrete elements was assumed in the FE model.

It is observed that Non-linear load-deflection curves show very close results at every stage of load history of the slabs up to failure. The FE analysis can trace the test results closely. The initially linear relation experience a small jump with a sudden loss of stiffness, when cracking in concrete begins followed by a nearly linear response with a decreased slope. The almost bilinear response of the FE model is consistent with the test data. Hence it may be concluded that the FE model can be used to predict the whole load-deformation curve which includes the elastic and the plastic part, flexural and shear cracking initiation, concrete crushing, and the yielding of the steel bars.

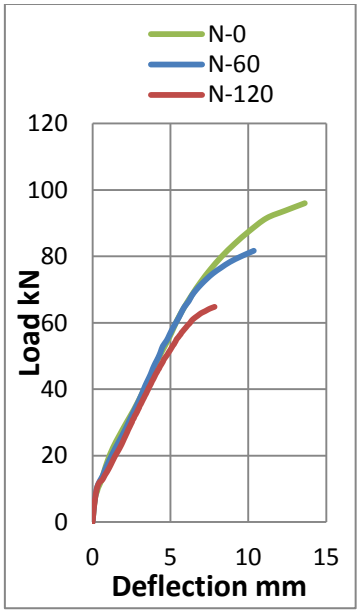


Figure 12: Load-deflection curves for NSC flat plate

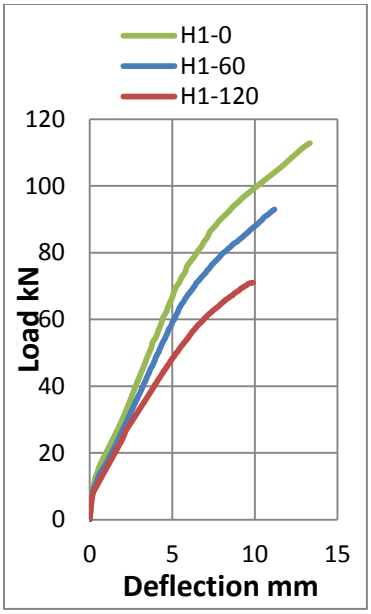


Figure 13: Load-deflection curves for 70 MPa flat plate

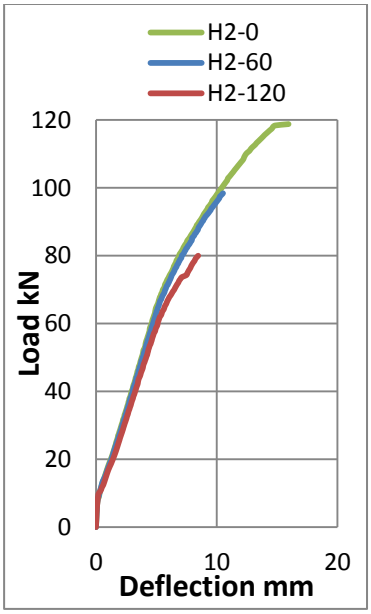


Figure 14: Load-deflection curves for 90 MPa flat plate

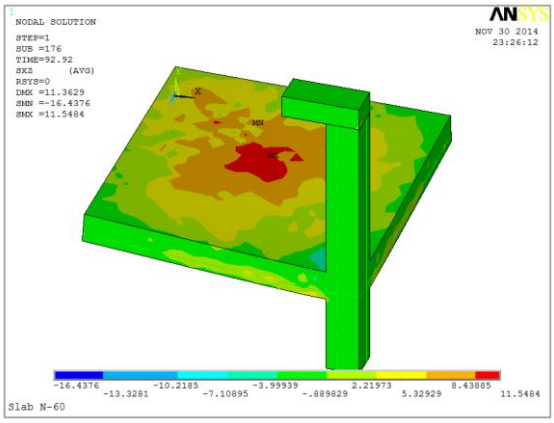


Figure 15: theoretical stress distribution for N-60

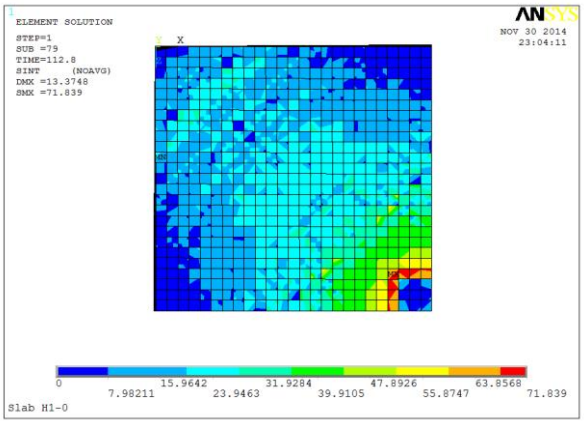


Figure 16: theoretical Strain distribution for H1-0

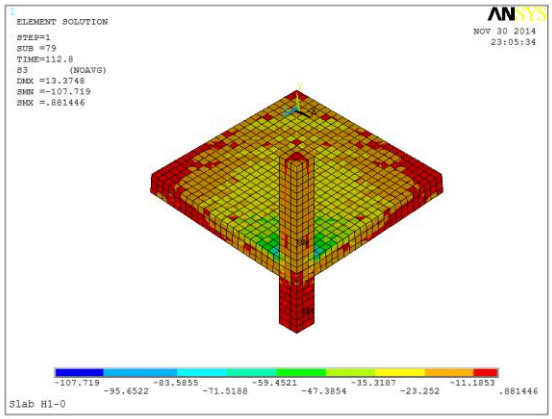


Figure 17: theoretical principle stress distribution for H1-0

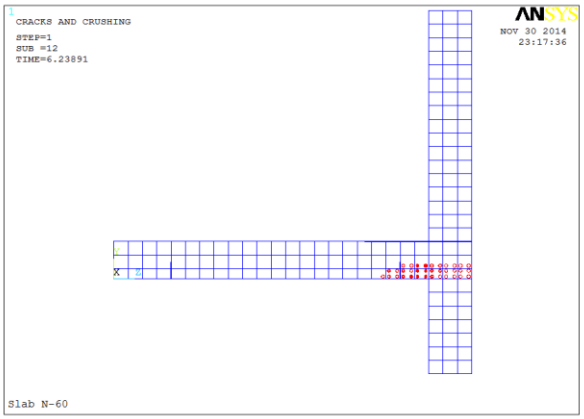


Figure 18: theoretical crack pattern for N-60

## 8. General Load Capacity and the Failure Mode

For the FE model, the ultimate load capacity for the slabs was considered as the highest converged load. Table 3 lists ultimate load capacity and first crack load for all tested slabs. The total stress and strain distribution for the slabs N-60 and H1-0 at failure stages are shown in Figures 15, 16 and 17 respectively. All the predicted ultimate punching load to experimental load were within (101%) in Table 3. The failure mode was punching shear around the column due to the stress concentration, for all test slabs.

## 9. First Cracking Load

In the FE model the first cracking load is defined as the load step where the first signs of cracking take place in the concrete elements solid65. Loads at first cracking in the model and in the experimentally tested beam are compared in Table 3. The theoretical crack pattern for N-60 is shown in Figure 18. The experimental first cracking loads to the FE model were within an average of 0.89 for the all slab specimens in Table 3. In all cases, the first cracking load from experimental data was higher than that from the FE model. This is possibly due to the experimental crack is the first visible one during the test, while in FE model the crack is taken place, at the sampling point within the element, when the first principal stress exceeds the tensile strength of the concrete.

## 10. Studying New Variable

After the FE model was modeled and verified in the previous section it has been used to study the effect of new variables on the behavior of RCFP under punching load. The new variables applied to the flat plate specimen with zero eccentricity (N-0, H1-0 and H2-0). The new variables are:

1- Increasing the flexural reinforcement ratio form (φ8@ 65 mm) to (φ10@ 65 mm) and (φ12@ 65 mm).

2- Adding extra top grid reinforcement (same as the bottom reinforcement) ((φ8@ 65 mm), in Figure 19.

3- Increasing the slab thickness by 10% (60mm) and 20% (66mm), in Figure 20.

Table 4 lists all the ultimate punching load capacity for the tested RCFP specimens per the new variables. It is clear that effect of increasing the reinforcement is insignificant, (101% – 102%). Also using top reinforcement grid increase the ultimate load capacity by not more than (104%). It is also obtained that increasing the total RCFP depth by (10%) and (20%) lead to increasing the ultimate load capacity by (15%) and (29%) respectively.

Table 4: The ultimate load capacity for the RCFP slab with new variables

| RCFP Specimen | Additional main flexural reinforcement (kN) | | | | Additional top reinforcement grid (kN) | | Increasing the total slab thickness (kN) | | | |
|---|---|---|---|---|---|---|---|---|---|---|
| | (φ10@ 65 mm) | | (φ12@ 65 mm) | | (φ8@ 65 mm) | | Total depth (60mm) | | Total depth (66mm) | |
| N-0 | 97.3 | 101% | 97.5 | 102% | 99.2 | 103% | 109.5 | 114% | 124.2 | 129% |
| H1-0 | 114.2 | 101% | 115 | 102% | 117.1 | 104% | 130.7 | 116% | 142.5 | 126% |
| H2-0 | 120.7 | 102% | 120.5 | 101% | 123.9 | 104% | 139.4 | 117% | 155.3 | 131% |

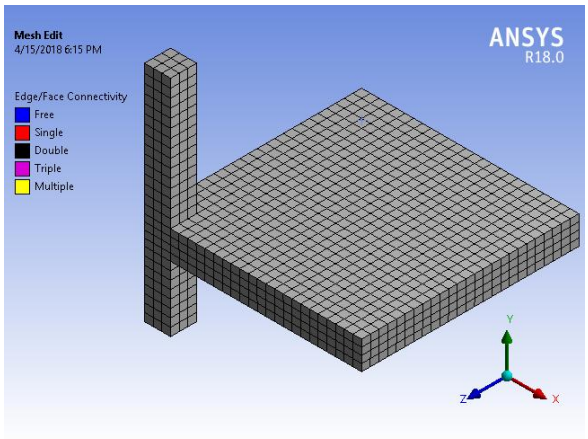


Figure 19: RCFP with 66mm total slab thickness

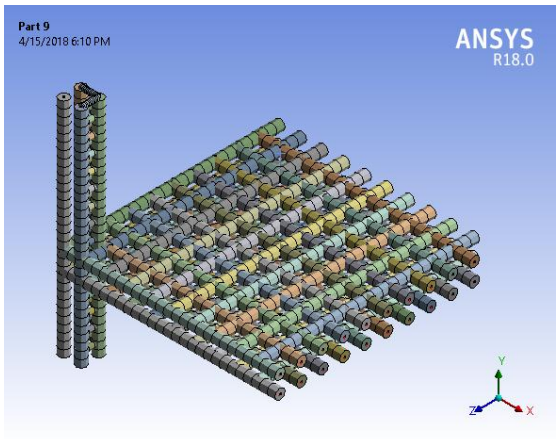


Figure 20: RCFP with top reinforcement grid

## 11. Conclusion

1. The FE model results show good agreement with the results of the experimental tests such as load-deflection curve, ultimate load, final deflection and mode of failure.
2. The FE model-ANSYS model which was modeled and calibrated can be used to study the effect

of new variables on the two-way shear (punching) of flat plate slabs, through applying the new variables to the model and re-analyzing it.

3. As the concrete strength increased from 40, 75 to 110 MPa, the average ($\frac{Pu\ Exp.}{Pu\ ANSYS}$) remained essentially the same (1.00). This means that the model is highly effective for all concrete strength.
4. The effect of reinforcement ratio is found insignificant (2%), on the punching load capacity. Approximately doubling the ratio (top mesh reinforcement) has only increased the capacity by maximum 4%.
5. The effect of slab thickness is found significant on the punching load capacity. Increasing the thickness by 10% and 20% has increased the capacity by 15% and 29%, respectively.

**References**

ACI 318M (2014). Building Code Requirements for Structural Concrete and Commentary, reported by ACI committee 318.

ACI Committee 363 (2013). State of the Art Report on High Strength Concrete, ACI Manual of Concrete Practice, Part 5.

ACI CT-13 (2013). ACI Concrete Terminology, ACI STANDARD, First Printing January 2013.

ANSYS (2016). ANSYS User's Manual Revision 5.5. ANSYS, Inc., Canonsburg, Pennsylvania.

Bangash, M. Y. (1989). *Concrete and Concrete Structures: Numerical Modeling and Applications.* London: Elsevier Science Publishers Ltd.

Darwish, A., & Yaseen, A. (2006). Punching strength resistance in steel fiber reinforced high strength concrete plates. M.Sc. Thesis, Univesity of Salahaddin, Iraq.

Desayi, P., & Krishnan S. (1964). Equation for the stress-strain curve of concrete. *Journal of the American Concrete Institute*, 6193), 345-350.

Elstner, R. C., & Hognestad, E. (1956). Shearing strength of reinforced concrete slabs. *ACI Structural Journal*, 28(1), 29-58.

Gere, J. M., & Timoshenko, S. P. (1997). *Mechanics of Materials*. Boston: PWS Publishing Company.

Nilson, A.H., Darwin, D., & Dolan, C.W. (2010). *Design of Concrete Structures*. 14th Ed., New York: McGraw Hill.

Tavarez, F. A. (2001). Simulation of Behavior of Composite Grid Reinforced Concrete Beams using Explicit Finite Element Methods. Master's Thesis, University of Wisconsin-Madison, Madison, Wisconsin.

Timoshenko, S. P., & Gere, J. M. (1997). *Mechanics of Materials*. Boston: PWS Publishing Company.